International Journal of Nanomedicine

Dovepress
open access to scientific and medical research

Open Access Full Text Article

ORIGINAL RESEARCH

Preparation and Evaluation of Doxorubicin-Loaded PLA–PEG–FA Copolymer Containing Superparamagnetic Iron Oxide Nanoparticles (SPIONs) for Cancer Treatment: Combination Therapy with Hyperthermia and Chemotherapy

This article was published in the following Dove Press journal:
International Journal of Nanomedicine

Mohammad Khaledian[1]
Mohammad Sadegh Nourbakhsh[1,2]
Reza Saber[3]
Hadi Hashemzadeh[4]
Mohammad Hasan Darvishi[5]

[1]Department of Biomedical Engineering, Faculty of New Sciences and Technologies, Semnan University, Semnan, Iran; [2]Faculty of Materials and Metallurgical Engineering, Semnan University, Semnan, Iran; [3]Research Center for Science and Technology in Medicine, Tehran University of Medical Sciences, Tehran, Iran; [4]Department of Nanobiotechnology, Faculty of Bioscience, Tarbiat Modares University, Tehran, Iran; [5]Nanobiotechnology Research Center, Baqiyatallah University of Medical Sciences, Tehran, Iran

Background: Among the novel cancer treatment strategies, combination therapy is a cornerstone of cancer therapy.

Materials and Methods: Here, combination therapy with targeted polymer, magnetic hyperthermia and chemotherapy was presented as an effective therapeutic technique. The DOX-loaded PLA–PEG–FA magnetic nanoparticles (nanocarrier) were prepared via a double emulsion method. The nanocarriers were characterized by particle size, zeta potential, morphology, saturation magnetizations and heat generation capacity, and the encapsulation efficiency, drug content and in-vitro drug release for various weight ratios of PLA:DOX. Then, cytotoxicity, cellular uptake and apoptosis level of nanocarrier-treated cells for HeLa and CT26 cells were investigated by MTT assay, flow cytometry, and apoptosis detection kit.

Results and Conclusions: The synthesized nanoparticles were spherical in shape, had low aggregation and considerable magnetic properties. Meanwhile, the drug content and encapsulation efficiency of nanoparticles can be achieved by varying the weight ratios of PLA:DOX. The saturation magnetizations of nanocarriers in the maximum applied magnetic field were 59/447 emu/g and 28/224 emu/g, respectively. Heat generation capacity of MNPs and nanocarriers were evaluated in the external AC magnetic field by a hyperthermia device. The highest temperature, 44.2°C, was measured in the nanocarriers suspension at w/w ratio 10:1 (polymer:DOX weight ratio) after exposed to the magnetic field for 60 minutes. The encapsulation efficiency improved with increasing polymer concentration, since the highest DOX encapsulation efficiency was related to the nanocarriers' suspension at w/w ratio 50:1 (79.6 ± 6.4%). However, the highest DOX loading efficiency was measured in the nanocarriers' suspension at w/w ratio 10:1 (5.14 ± 0.6%). The uptake efficiency and apoptosis level of nanocarrier-treated cells were higher than those of nanocarriers (folic acid free) and free DOX-treated cells in both cell lines. Therefore, this targeted nanocarrier may offer a promising nanosystem for cancer-combined chemotherapy and hyperthermia.

Keywords: combination therapy, doxorubicin, hyperthermia, magnetic nanoparticles, targeted drug delivery

Introduction

Cancer is a major public health issue with increasing incidence and mortality. There are many types of cancer treatment approaches such as immunotherapy, radiotherapy, and surgery. Following surgery, the chemotherapy is considered as the convenient treatment

Correspondence: Mohammad Hasan Darvishi
Email Darvishi@alumnus.tums.ac.ir

submit your manuscript | www.dovepress.com
DovePress
http://doi.org/10.2147/IJN.S261638

approach for cancer. However, conventional chemotherapy is limited due to its low bioavailability and severe side-effects, such as cardiotoxicity.[1–3] In recent years, developing nanocarrier platforms for drug delivery (chemical agent, protein, DNA, siRNA) with multifunctional ability, such as combined therapy (eg simultaneous hyperthermia and chemotherapy), targeted drug delivery and stimuli-controlled release, were considered more attractive approaches in disease treatment.[2,4–13] Compared with conventional formulations, the therapeutic agents encapsulated in nanoparticles possess characteristics of desired solubility, enhanced bioavailability and selective biodistribution endowed by their carriers.[13–16] Among the carriers, the nanoparticles (NPs) prepared from poly (lactide) (PLA) have been extensively used due to its biocompatible, biodegradable and nontoxicity features.[17–19] Further modification of PLA with poly (ethylene glycol) (PEG) could enhance systemic retention, since it can reduce nonspecific protein adsorption, opsonization and subsequent clearance by the reticuloendothelial system (RES).[19,20] It has also been shown that the high water content of PEG increases the diffusion of water into the copolymer system and causes faster hydrolysis of nanoparticles.[21] However, one major limitation of PLA-NPs is that it cannot differentiate the cancerous cells from normal cells. Targeted drug delivery can be achieved by adding different groups and ligands, such as aptamers,[22,23] antibodies,[24,25] peptides[25,26] and vitamins[9,27,28] to nanoparticles. Meanwhile, small ligands of the vitamin molecule, such as folic acid, due to the fact that they do not significantly increase the size of the nanoparticle, as well as developing more stable connections with nanoparticles, are more noteworthy.[11,29] Also, folate receptors have a high expression level in many cancer cells than healthy cells.[30,31] In fact, due to overexpression of vitamin receptors such as folate in cancer cells than healthy cells, penetration drug delivery systems into tumor cells facilitated by this phenomenon. The folic acid linked-nanocarriers could further enhance the accumulation level and drug release rate in tumor area reported in a previous study by Daglioglu.[32] Therefore, folic acid conjugated polymers can be used to increase the specificity and cellular uptake of anti-cancer drugs in tumor cells through receptor-mediated endocytosis by folate receptors.[33,34] Doxorubicin (DOX) is one of the most effective antitumor drugs for solid tumors including breast, ovarian, lung and prostatic cancers.[35–38] Loading of doxorubicin in nanoparticles increases its bioavailability and anti-tumor activity, DNA affinity and reduces its severe side-effects.[39–41]

The idea of combined therapy by mixing more than two therapeutic agents in the form of a multifunctional nanoparticle platform has been introduced as a strategy to gain synergistic effects of therapeutic agents on disease treatment.[42,43] Hyperthermia or thermal therapy, ie raising the temperature of tumor tissues to 40–45°C, has provided acceptable benefits and is a promising approach for cancer treatment.[44–46] At this temperature range, heat inhibits the regulatory and growth processes of cancerous cells. Heating tumors to above physiological temperatures is not only cytotoxic but also activates several mechanisms by which tumor cells are sensitized to the primary treatment.[47,48] Magnetic hyperthermia is a particularly attractive medical therapeutic approach, which is based on the inductive heating of magnetite nanoparticles (SPIONs) under the application of an alternating magnetic field (AMF).[47,49] The inevitable technical problem of hyperthermia is the difficulty in heating only the local tumor region to the intended temperature, without damaging the surrounding healthy tissue. Magnetic iron oxide nanoparticles can offer opportunities toward developing an effective local hyperthermia effect. If Fe_3O_4 nanoparticles could be made to accumulate only in the tumor tissue, cancer-specific hyperthermia would be achieved by generating heat in an AC magnetic field.[50–52] Therefore, magnetic hyperthermia in association with chemotherapy offers novel insight with more efficacy in cancer treatment and is a route for overcoming the limitations of drug resistance and off-target hyperthermia.

In this study, DOX-loaded PLA–PEG–FA SPIONs for targeted co-delivery of DOX and SPIONs into tumor cells is investigated. The physicochemical properties of DOX-loaded PLA–PEG–FA SPIONs such as size, zeta potential, morphology and magnetization were assessed. The encapsulation efficiency, loading capacity and DOX release from the DOX-loaded PLA–PEG–FA SPIONs were evaluated. The cytotoxicity, cellular uptake and apoptotic effect of DOX-loaded PLA–PEG–FA SPIONs were evaluated quantitatively using MTT and flow cytometry in two cell lines including HeLa and CT26 cells. Furthermore, an in-vitro hyperthermia experiment under AMF for DOX-loaded PLA–PEG–FA SPIONs was performed (Schematic diagram 1).

Schematic diagram1. A) Schematic structure of multifunctional nanocarriers and cancerous cells-targeted for B) combined thermotherapy and chemotherapy by DOX-loaded PLA–PEG–FA SPIONs nanocarriers under alternating magnetic field (AMF).

Materials and Methods

Materials

$FeCl_3.6H_2O$, $FeCl_2.4H_2O$, N,N′-dicyclohexylcarboiimide (DCC), N-hydroxysuccinimide (NHS), Folic Acid, α-Amine

-ω-hydroxy PEG (Mw 3000 Da), D, L-lactide, stannous-2-ethyl-hexanoate, fluorescein isothiocyanate (FITC)-labeled phalloidine, 3-(4, 5-dimethyl-2-thiazolyl)-2 and5-diphenyl -2-H-tetrazolium bromide (MTT) were obtained from Sigma-Aldrich (St. Louis, MO, USA). Doxorubicin (DOX) was purchased from RPG Life Sciences limited (Mumbai, India). AnnexinV-APC/7-AAD double labeling kit was obtained from BD Bioscience (5 mL per test, San Jose, CA, USA). Cell culture media, fetal bovine serum (FBS) and 0.25% trypsin were purchased from Gibco BRL (Carlsbad, CA, USA). All used cells were purchased from the National Cell Bank of Iran (NCBI).

Synthesis of Superparamagnetic Iron Oxide Nanoparticles (SPIONs)

Magnetite nanoparticles were synthesized by co-precipitation of $FeCl_2 \cdot 4H_2O$ and $FeCl_3 \cdot 6H_2O$ in a molar ratio of 1:2.[53] Briefly, 0.7 g $FeCl_2.4H_2O$ and 1.4 g $FeCl_3.6H_2O$ dissolved in 50 mL of deionized water, heated to 70°C under nitrogen gas. After stirring (10 min), sodium hydroxide was added to the mixture, and then the suspension was cooled and the precipitates were separated by magnetic decantation with ethanol and distilled water. The subsided Fe_3O_4 nanoparticles were dried in a vacuum atmosphere at 60°C.

Synthesis of PLA–PEG–FA Conjugates

Synthesis of NHS-Folic Acid

To synthesize the NHS-folic acid, first, an anhydrous dimethyl sulfoxide (DMSO, 40 mL) and triethylamine (TEA, 0.5 mL) mixture was prepared, and then folic acid (0.5 g) was added to the mixture. The reaction solution was stirred at room temperature for 24 hrs in dark-room conditions. Then, a mixture of dicyclohexylcarbodiimide (DCC, 0.2 g) and n-hydroxysuccinimide (NHS, 0.14 g) was added to the reaction solution and stirred in dark-room conditions for further 24 hrs. The DMSO and TEA substances were vaporized under a vacuum.

Preparation of FA–PEG–OH

A solution of α-Amine-ω-hydroxy PEG (0.1 g) dissolved in dried acetonitrile (0.2 mL) was prepared. Dichloromethane (DCM, 0.1 mL) and triethylamine (TEA, 10 µL) were added to the above solution and stirred at room temperature for 1 min. NHS-FA (0.02 g) was introduced to the above reaction mixture and stirred overnight under nitrogen. The reaction was stopped by slightly adding diethyl ether to precipitate the polymer and to separate the unreacted PEG. Precipitated polymers were then dissolved in hot 2-propanol (70°C). The resulting cloudy solution was re-precipitated by cooling and the unconjugated folic acids were removed by dialysis (MWCO 1000). The final product was lyophilized and then analyzed by ^{1}H-NMR and FTIR spectroscopy.

Preparation of PLA–PEG–FA

The solvent polymerization technique was applied to graft polymerization of lactide onto folic acid–PEG–OH. The co-polymers of PLA–PEG–FA were synthesized using previously reported with some modifications.[54] Glassware were salinized by rinsing with a 5% methyl trichlorosilane solution in toluene, followed by rinsing with acetone, and left overnight to dry at 130°C. FA–PEG–OH (0.05 g) and L-lactide (0.5 g) were added to a round bottom flask and diluted with 30 mL of dried toluene. The flask was heated to 60°C to dissolve the contents. After approximately 70% of the added toluene was removed, stannous-2-ethyl-hexanoate in toluene (25 mg in 0.2 mL) was added to the above reaction mixture and refluxed at 110°C for 4 hrs under nitrogen. Residual solvent was removed under vacuum condition using a rotary evaporator. The reaction mixture was cooled and dissolved in 2 mL dichloromethane. The polymer solution was then gradually added to a stirred solution of 3 mL chilled diethyl ether. The final polymer conjugate was isolated by vacuum filtration and then lyophilized. Finally, the conjugation was verified by FTIR and H-NMR spectroscopy.

Preparation of DOX-Loaded PLA–PEG–FA SPIONs

The DOX-loaded PLA–PEG–FA SPIONs were prepared by a double emulsion method.[54] Briefly, 1 mL water solution containing 10 mg SPIONs and 1.4 mg DOX was added drop-wise into 1 mL dichloromethane containing 14, 28, 70 mg PLA–PEG–FA copolymer (PLA–PEG–FA/DOX at various w/w ratios 10:1, 20:1, 50:1), and then the two-phase mixture was subjected to sonication for 30 s (70 w) in an ice bath. Subsequently, 4 mL of PVA solution (3% w/v) was added and sonicated for 30 s to form a w/o/w double emulsion and then stirred for 10 min. The resulting double emulsion was diluted by mixing with 50 mL of a 0.3% (w/v) PVA aqueous solution under vigorous stirring for 5 min, and then the organic solvent was evaporated using a rotary evaporator. In turn, nanoparticles were centrifuged at 13,000 rpm for 20 min, washed with deionized water and lyophilized.

Characterization of SPIONs and DOX-Loaded PLA–PEG–FA SPIONs

The particle size and surface charge of the SPIONs and DOX-loaded PLA–PEG–FA SPIONs were calculated by DLS (Malvern Zeta sizer 3000HS, Malvern, UK). The intrinsic magnetic properties of the SPIONs were measured by generating a magnetic hysteresis loop using a vibrating sample magnetometer (VSM; Weistron) in a magnetic field strength of ±10 kOe. The temperature-dependent magnetization of the sample was obtained by measuring the magnetization at a temperature level of 298 K with a maximum applied field of ±10 kOe. TB could be read from the ZFC and the FC curves taken under the applied magnetic field of 1000 Oe and temperature level of 298 K. The composition of the SPIONs and PLA–PEG–FA copolymer was characterized by H NMR^1 and FT-IR. The H NMR^1 spectra were obtained in D_2O using a 500 MHz spectrometer (Bruker Ac 500, Germany). The FTIR spectra (Nicolet 550 A, USA) were used to further confirm the structure of the resulted conjugates in each step. In addition, transmission electron microscopy (TEM; Model H-800, Hitachi, 200 kV, Tokyo, Japan) was applied to characterization and investigation of the morphology of the DOX-loaded PLA–PEG–FA SPIONs.

Investigating of Heat Generation Capacity

Heat generation capacity of SPIONs and DOX-loaded PLA–PEG–FA SPIONs were evaluated in the external AC magnetic field by a hyperthermia device (nanosys pars).[55] Briefly, magnetic fluid was prepared from SPIONs and DOX-loaded PLA–PEG–FA SPIONs with different concentrations (10, 15 and 20 mg/mL) in 2 mL deionized water. Then, each sample was placed inside the coil and magnetic field strengths were applied with 9.23 kA/m and field frequencies of 400 kHz. The heat generated by the particles was recorded and photographed by a thermal camera.

Evaluation of Encapsulation Efficiency

The encapsulation efficiency (EE) was defined as the percentage of the total drug entrapped. For this purpose, freeze-dried nanoparticles were dissolved in DMSO, and then the supernatant was collected by centrifugation. The concentration of DOX in the supernatant was measured by UV spectrophotometry (Varian, Cary 100 UV/Vis Spectrophotometer, USA) at 480 nm. The drug loading and encapsulation efficiency of DOX were calculated by the following formulas:[56]

$$\text{Drug loading content}(\%) = \frac{\text{the weight of DOX in the nanoparticles}}{\text{the gross weight of the nanoparticles}} \times 100$$

$$\text{Encapsulation efficiency}(\%) = \frac{\text{the weight of DOX in the nanoparticles}}{\text{the total weight of the feeding DOX}} \times 100$$

In-vitro Release Study

To investigate the drug release behavior of the nanoparticles in physiological environments, the dialysis bag diffusion technique was used. To this end, DOX-loaded PLA–PEG–FA SPIONs were transferred into a dialysis bag (molecular weight cutoff 12 kDa), and the bag was immersed in a receiver compartment (PBS) at pH 7.4. The release system was kept in an incubator shaker (Taitec, BR-42FL, Japan) at 37°C and 100 rpm to provide a sink condition. Samples were withdrawn from the receiver medium at time intervals of 0.5, 1, 2, 4, 8, 12, 24 and 48 hrs, and then were replaced with equal volumes of fresh PBS. The released drug value was determined at 480 nm by a UV/Vis spectrophotometer.

Cell Line Experiments

Cell Culture

HeLa (human cervix epithelial carcinoma cells) and CT26 (colon carcinoma cell) were cultured in RPMI 1640 (Gibco, BRL, USA), supplemented with 10% FBS (Gibco), streptomycin (100 ng/mL), and penicillin (100 U/mL) at 37°C in a 5% humidified CO_2 incubator. The cell lines were purchased commercially from the National Cell Bank of Iran (NCBI) at Pasteur Institute of Iran.

In-vitro Cytotoxicity

In-vitro cytotoxicity assay of the DOX-loaded PLA–PEG–FA SPIONs was performed by an MTT assay. The cells were seeded at an initial density of 1×10^4 cells/well of growth medium in 96-well plates and incubated for 24 hrs to reach 70–80% confluences. Cells were then incubated with DOX-loaded PLA–PEG–FA SPIONs at various w/w ratios 10:1, 20:1, 50:1 (PLA–PEG–FA:DOX). Untreated cells, free DOX-treated and PLA–PEG–FA SPION-treated cells were used as controls. After incubation for 24 hrs at 37°C, the supernatant was removed, and the cells were washed with PBS three times. Then, 10 µL of 5 mg/mL MTT salt in PBS was added into each well and the plates were incubated for 4 hrs in a 5% CO_2 humidified atmosphere at 37°C. Afterwards, the medium was removed and 100 µL of DMSO was added to each well and the plates

were shaken for 15 min to dissolve the formazan crystals. Finally, the absorbance was measured at 570 nm using the microplate reader (Stat Fax 2100, Block Scientific, USA). The cell viability was calculated by the following equation:

$$\text{cell viability} = \frac{\text{absorption value of treatment group}}{\text{absorption value of control group}}$$

Flow Cytometry

The cellular uptake of DOX-loaded PLA–PEG–FA SPIONs was evaluated in HeLa and CT26 cells using flow cytometry and fluorescence microscopy. For the flow cytometry, the cells were seeded in 12-well plates in 1 mL of growth medium at the initial density of 5×10^4 cells per well and cultured for 24 hrs. The medium was then changed with a 1 mL fresh suspension containing different samples. Then, the cells were collected and washed three times with PBS for analyzing the DOX fluorescence intensity using a FACS caliber flow cytometer (Becton Dickinson Immunocytometry Systems, San Jose, CA). Moreover, cellular internalization of the DOX-loaded PLA–PEG–FA SPIONs and free DOX were analyzed by a fluorescence microscope (Leica Microsystems Inc., Buffalo Grove, IL). To identify necrosis and apoptosis, the Annexin V-FITC apoptosis detection kit was used. Briefly, the cells were incubated with the different samples for 24 hrs. Then, the cells were harvested, centrifuged and washed with PBS. Afterwards, the cells were re-suspended in 100 µL of binding buffer containing 5 µL FITC-labelled annexin V and incubated for 20 min at ambient temperature in a dark room. Finally, the cells were examined using a FACS caliber flow cytometer (Becton Dickinson Immunocytometry Systems, San Jose, CA).

Statistical Analysis

To statistical analysis, all data such as MTT assay, apoptosis were subjected to analysis of variance (one-way ANOVA multiple comparisons). The means were compared using Tukey's multiple comparisons test at $p = 0.05$. The means ± SE were used to compare the data using GraphPad Prism software (version 8.0.2, Prism Corporation Pvt Ltd, San Diego, CA, USA).

Results and Discussion

Preparation and Characterization of SPIONs

Superparamagnetic iron oxide nanoparticles were synthesized by the co-precipitation method as reported in our previous work. The FTIR spectrum of dispersed Fe_3O_4 nanoparticles in de-ionized water is given in Figure 1. The peak observed at around 3415.53 cm^{-1} is due to O–H stretching vibration arising from hydroxyl groups from the water on nanoparticles. The absorption peaks at 2921.10, 1623.87, 1385.35 and 1054.49 cm^{-1} are related to de-ionized water used as the solvent. Considering the IR spectra of Fe_3O_4 nanoparticles, the 517.09 cm^{-1} absorption peaks belong to the Fe–O bond vibration of SPIONs nanoparticles. The average size of synthesized SPIONs nanoparticles is 41/98±3 nm with relatively uniform size distribution (PDI: 0/16±0/01), zeta potential observed equal to −28/3±2/5 mV at pH 7.0. Suspension of prepared Fe_3O_4 nanoparticles did not contain large aggregates and was stable for 8 weeks without obvious changes in magnetic properties. The stability of iron nanoparticles depends on particle size, surface condition and environment. The SPIONs nanoparticles become chemically unstable in the aqueous solution, especially when they are small and have a hydrophilic surface.

Synthesis and Characterization of PLA–PEG–FA

The PLA–PEG copolymer was synthesized using the ring-opening polymerization method.[57] The FTIR spectra of PEG–FA and PLA–PEG–FA are shown in Figure 1. Considering the FT-IR spectra of PEG–FA, the new amide peaks appeared at around 1697.59 cm−1 ((C=O) in saturated amide bond), implying that carboxylic acid groups of folic acid successfully reacted with primary amines of PEG. After grafting PLA to the FA–PEG–OH, the peak at 1344.89 cm^{-1} (which is related to the hydroxyl groups of PEG) disappeared and the ester peak appeared at 1754.05 cm^{-1}((C=O) in saturated ester bond) indicating that carboxylic acid groups of PLA successfully reacted with OH group of PEG. In addition, presence of indicator peaks for folate (1604/33 cm^{-1} (aromatic), 1697/36 cm^{-1} (C=O)), PEG (1186/05 cm^{-1} (C-O), 2938/32 cm^{-1} (C-H)) and PLA (1730/3 cm^{-1} (C=O)) have confirmed synthesis of PLA–PEG–FA co-polymer. The H NMR^1 of PEG–FA and PLA–PEG–FA copolymer is shown in Figure 2. The strong peaks around 3–3.5 ppm correspond to the CH_2 protons of PEG. The small peak at 5.2 ppm belongs to the CH_3 protons of PLA. The peaks at 4.5, 6.75, 7.5, and 8.75 ppm correspond to the presence of folate ring protons. The H NMR^1 spectrum indicates the ring-opening polymerization of lactide and formation of block copolymer.

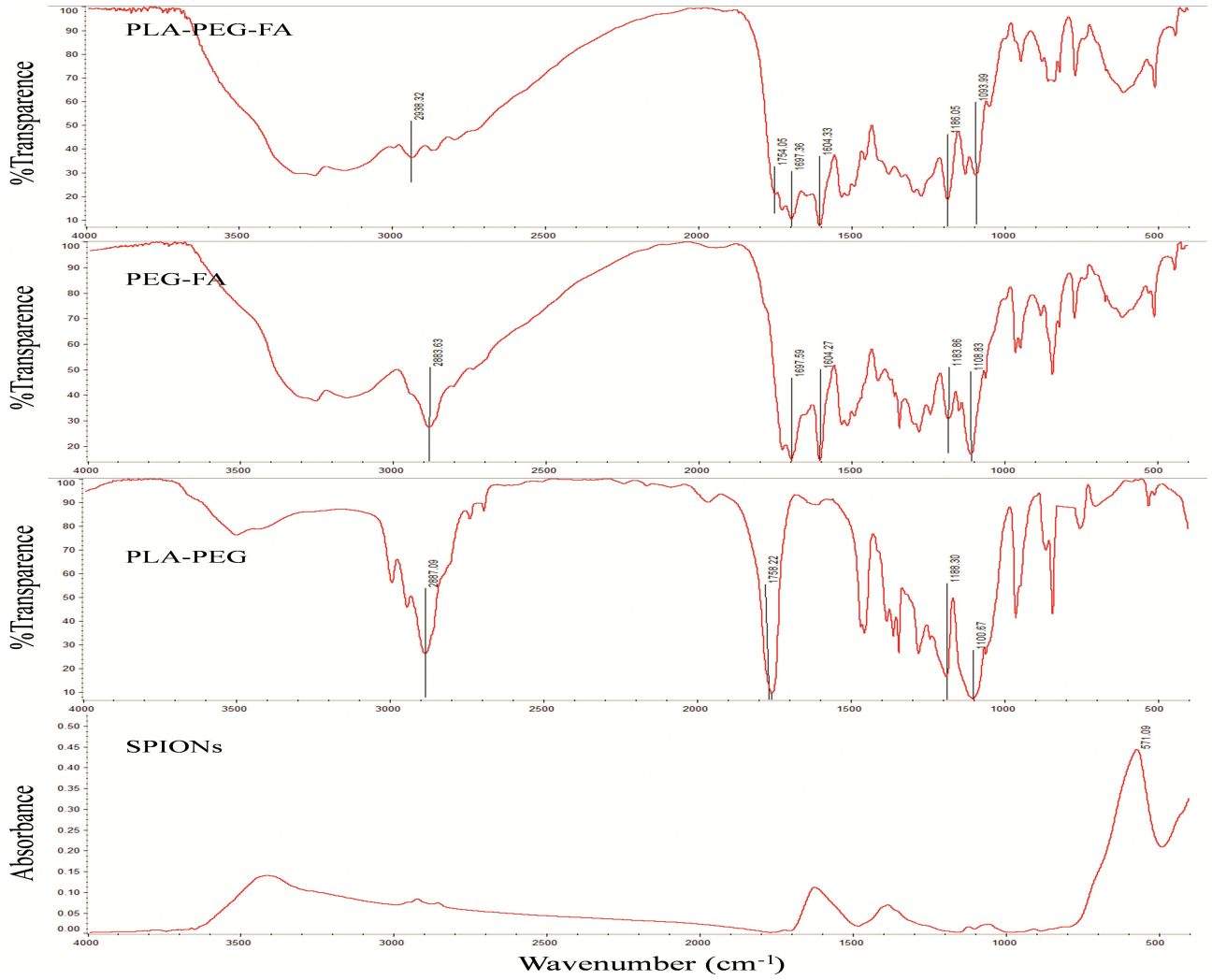

Figure 1 The FTIR spectra of (**A**) PLA–PEG–FA (**B**) PEG–FA (**C**) PLA–PEG Co-polymers and (**D**) superparamagnetic iron oxide nanoparticles (SPIONs).

Preparation and Characterization of DOX-Loaded PLA–PEG–FA SPIONs

Size, Zeta Potential and Morphology

The DOX-loaded PLA–PEG–FA SPIONs nanoparticles were prepared using the double emulsion (W/O/W) method.[57] Physicochemical properties of the prepared nanoparticles such as size, zeta potential, and morphology were investigated. The particle sizes of DOX-loaded PLA–PEG–FA SPIONs at various w/w ratios (PLA–PEG–FA:DOX) 10:1, 20:1, 50:1 (w/w) were assessed by dynamic light scattering (DLS), tabulated in Table 1. The particle size ranged between 71.13 and 257.1 nm, with a constant increase according to an increase in their w/w ratios. Nanoparticles size increase can be attributed to the swelling of the polymer coating on the surface of the nanoparticles upon DOX encapsulation. TEM analysis (Figure 3) revealed that the nanoparticles were fairly smooth and are of spherical shape, and the average size at 10:1 ratio (w/w) was 32 nm. The difference between the obtained size results is related to the fact that DLS yields a larger size value due to measuring the hydrodynamic diameter of the particle while including the solvation layers, whereas, in TEM analysis, nanoparticles could potentially dehydrate and shrink during TEM sample preparation and thus resulting in lower nanoparticle diameter.[58] The zeta potential of DOX-loaded PLA–PEG–FA SPIONs at various ratios were in the range of −22.9 (w/w ratio 10:1) to −25.6 mV (w/w ratio 50:1). These surface charges increased with the w/w ratio (Table 1). The zeta potential values of the prepared DOX-loaded PLA–PEG–FA SPIONs were not affected by the encapsulation of DOX (Data are not shown). The size and surface charge are important physiochemical parameters in the development of nanoparticles-based delivery systems. These properties could

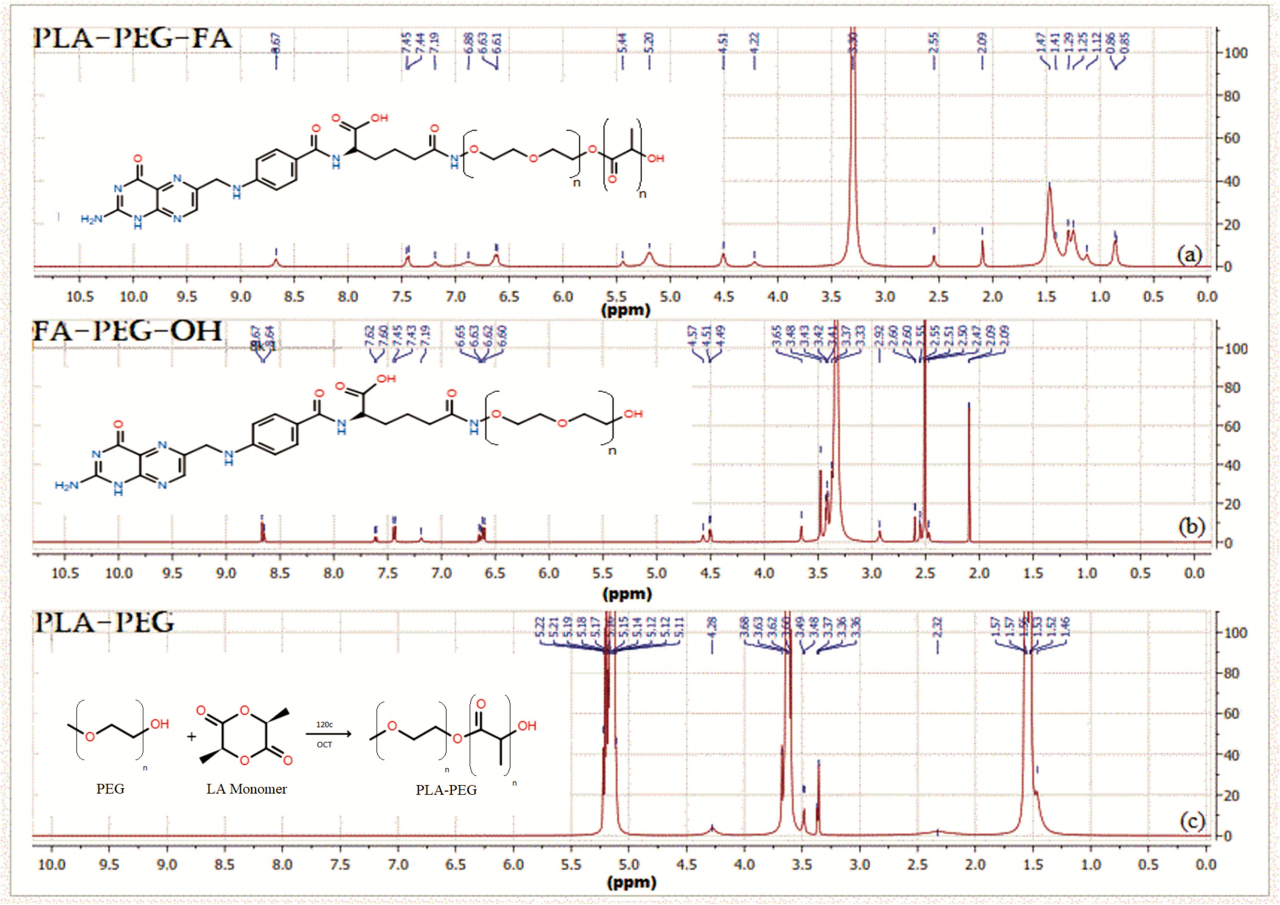

Figure 2 ^{1}H-NMR spectra of (**A**) PLA–PEG–FA (**B**) FA–PEG–OH and (**C**) PLA–PEG Copolymers.

influence the half-life of the NPs in blood circulation, the interactions between the NPs and cell surface, uptake, and finally their cellular uptake efficiency.[59] The formation of core/shell structures was confirmed by TEM analysis (Figure 3). The core-shell system maintains the morphological features of SPIONs and the desired size range. The hydrophobic PLA chain tendency is to be inserted into the surface of SPIONs while hydrophilic PEG chain extending outside. This polymeric shell is expected to protect the magnetic core from oxidation in physiological conditions, thus improving the stability of SPIONs. The hydrophilic nature of the shell can also prevent the adsorption of protein on the surface of the delivery system through steric repulsion and then escape the capture by the RES and extend their fate in the circulatory system. However, the thickness of the shell is critical for obtaining the saturation magnetization strength and subsequently the heat generation potential of SPIONs nanoparticles. Our TEM analysis results showed that the resulting core/shell nanoparticles were fairly uniform in size distribution and with a thin shell.

Magnetic Properties

The magnetic properties of the SPIONs and DOX-loaded PLA–PEG–FA SPIONs at ratio 10:1 (w/w) were

Table 1 Size, Zeta Potential and PDI of Nanoparticles

Sample	Z-Average± SD (d.nm)	PDI ± SD	Z Potential ± SD(MV)
SPIONs	41.98±2.6	0.16±0.01	−28.3±2.5
DOX-loaded PLA–PEG–FA SPIONs (10:1)	71.13±3.5	0.37±0.03	−22.9±1.1
DOX-loaded PLA–PEG–FA SPIONs (20:1)	140.5±8.5	0.44±0.03	−25.2±1.7
DOX-loaded PLA–PEG–FA SPIONs (50:1)	257.1±13	0.45±0.02	−25.6±2.2

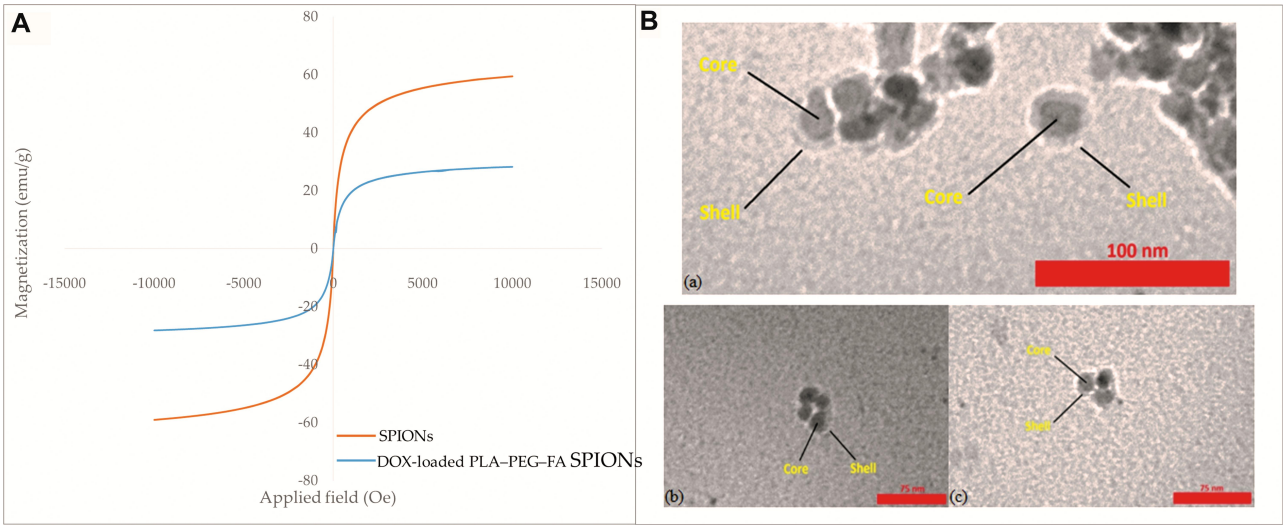

Figure 3 (**A**) Hysteresis loops for SPIONs and DOX-loaded PLA–PEG–FA SPIONs (at w/w ratio10:1) and (**B**) TEM images of DOX-loaded PLA–PEG–FA SPIONs (at w/w ratio 10:1).

investigated by VSM analysis. The hysteresis curves for SPIONs and DOX-loaded PLA–PEG–FA SPIONs are shown in Figure 3. The saturation magnetizations (Ms) of SPIONs and DOX-loaded PLA–PEG–FA SPIONs in the maximum applied magnetic field were equal to 59/447 emu/g and 28/224 emu/g, respectively. The SPIONs and DOX-loaded PLA–PEG–FA SPIONs exhibited superparamagnetic behavior without magnetic hysteresis. Due to the presence of DOX and PLA–PEG–FA, the saturation magnetization of DOX-loaded PLA–PEG–FA SPIONs was lower than the SPIONs. Nonetheless, the magnetization value of DOX-loaded PLA–PEG–FA SPIONs is sufficient for hyperthermia applications. Therefore, this result shows that magnetic properties of SPIONs are basically preserved in DOX-loaded PLA–PEG–FA SPIONs at 10:1 ratio under an external magnetic field.

Heating Properties of the Delivery System: In-vitro Hyperthermia

The heat generation property of magnetic nanoparticles is mainly due to hysteresis loss.[60] In addition, other parameters such as size and concentration of magnetic nanoparticles, magnetic field intensity, and the application time of magnetic field also considerably influence the heating properties under AC magnetic fields. The optimum temperature for most mild hyperthermia applications is in the 40–45° C range and requires durations of 30–60 min.[61] In the conducted hyperthermia experiments herein, different concentrations of magnetic nanoparticles were exposed to the AC magnetic field for 5 and 60 min. By increasing both the concentration of SPIONs and the AC magnetic field exposure time, the temperature of the suspensions containing SPIONs gradually increased up to 43.1° C and 48.2° C (Table 2). Meanwhile, in suspensions containing DOX-loaded PLA–PEG–FA SPIONs, the heating behaviors of SPIONs are affected by their concentration, the AC magnetic field exposure time and amount of PLA–PEG–FA in the particles. The presence of coatings can reduce the heating properties of the synthesized SPIONs. In the suspensions containing DOX-loaded PLA–PEG–FA SPIONs, only 10:1 ratio (w/w) at concentrations of 15 mg/mL and 20 mg/mL of SPIONs were capable to produce sufficient heat for hyperthermia. The highest temperature, 44.2° C, was measured in the DOX-loaded PLA–PEG–FA SPIONs suspension after exposed in the magnetic field for 60 min. Decrease in the temperature of suspensions containing DOX-loaded PLA–PEG–FA SPIONs at 10:1 ratio w/w, is in good agreement with the magnetization studies, which showed that drug loading and surface coating with PLA–PEG–FA copolymer slightly decrease magnetic moments of SPIONs. However, the temperature of suspensions containing DOX-loaded PLA–PEG–FA SPIONs at w/w ratios 20:1 and 50:1 was insufficient for hyperthermia due to the presence of coatings, even at 20 mg/mL concentration of SPIONs after 60 min. Therefore, it can be concluded that in core/shell structures such as DOX-loaded PLA–PEG–FA SPIONs, coating thickness has a decisive role in the success of hyperthermia.

Encapsulation Efficiency and Drug Loading

In this study, the multifunctional nanoparticles were prepared by a double emulsion method. Different factors,

Table 2 Heating Properties of SPIONs and DOX-Loaded PLA–PEG–FA SPIONs

Sample SPIONs Concentration (mg/mL)		Time (min)		Temperature (°C)	
		Min	Max	Min	Max
SPIONs	10	5	60	32.2±3.5	40.1± 3.0
	15	5	60	37.1±1.8	43.1± 2.4
	20	5	60	41.1± 2.0	48.2± 2.8
DOX Loaded PLA–PEG–FA SPIONs (10:1)	10	5	60	30.1± 3.1	34.1± 2.0
	15	5	60	32.3± 2.2	39.1± 3.1
	20	5	60	39.1± 2.5	44.2± 1.4
DOX Loaded PLA–PEG–FA SPIONs (20:1)	10	5	60	26.1± 1.0	32.1± 2.2
	15	5	60	32.1± 2.8	34.6± 2.6
	20	5	60	37.2± 3.2	40.2± 3.4
DOX Loaded PLA–PEG–FA SPIONs (50:1)	10	5	60	26.0± 1.4	31.2± 3.4
	15	5	60	29.5± 2.5	34.1± 1.4
	20	5	60	36.5± 2.8	38.5± 2.0

such as stirring speed and/or time, polymer concentration and stabilizer concentration, can significantly regulate and optimize the encapsulation of drugs for systems based on double emulsion techniques. Furthermore, encapsulation efficiency (EE) and drug content (LC) strongly depend on the w/w ratio of PLA–PEG–FA and DOX. In this study, at 10:1 w/w ratio, the EE was only 50.4 ± 2.5%, while at 50:1 w/w ratio, the encapsulation efficiency increased to 79.1 ± 4.5% (Table 3). The result indicated that the EE increases with polymer concentration. This observation is in agreement with the work of Ghasemi et al,[57] which found that higher polymer content resulted in higher encapsulation efficiency. This phenomenon can be possibly explained by the fact that in higher concentrations, the polymer precipitates faster and prevents drug diffusion across the polymer solution. Moreover, higher concentrations of polymer could lead to the higher viscosity of the solution and therefore delay drug diffusion within the polymer droplets. On the other hand, the loading efficiency was found to significantly decrease with the PLA–PEG–FA ratio (Table 3). The DOX loading level for 50:1 w/w ratio was 1.73± 1.3%. However, in 10:1 w/w ratio, the drug loading efficiency increased to 5.14 ± 0.40%. It seems that DOX can be efficiently incorporated into the polymer layers by simply mixing the polymer with the appropriate amount of the drug. Consequently, in DOX-loaded PLA–PEG–FA SPIONs, DOX was loaded into the hydrophobic polymer layers and the hydrophilic SPIONs were encapsulated into the inner aqueous core of the nanoparticles.

In-vitro Drug Release Study

To assess the potential of the developed cargo nanosystem as a drug carrier, the release profiles of doxorubicin from multifunctional nanoparticles were evaluated for 120 hrs at 37° C. DOX release profile from DOX-loaded PLA–PEG–FA SPIONs with different w/w ratios is illustrated in Figure 4. Compared with the free DOX that released to the extent of 92% within 2 hrs, the DOX-loaded PLA–PEG–FA SPIONs showed sustained release at a steady rate of DOX by diffusing through the polymeric matrix for 120 hrs. However, a small burst release occurred in the first 2 hrs (about 20% of the total loaded drug), followed by a slow drug release. About 90% of the total DOX loaded in DOX-loaded PLA–PEG–FA SPIONs at 10:1 w/w ratio was gradually released up to 120 hrs. In contrast, 65% and 68% of the total DOX were controlled release from the nanoparticles at w/w ratios 20:1 and 50:1, respectively. Fu et al[62] suggested that the drug release involved two different mechanisms of drug molecules diffusion and polymer matrix degradation. The burst release was probably related to the excess drug particles (close to the nanoparticles surface) dispersing rapidly from matrix into buffer in the first few hours. On the other hand, most DOX were relatively far from the nanoparticles surface as the polymer concentration increases. This might be one of the reasons for no obvious burst release of drug for such nanoparticles. As the results showed, with the increase in polymer concentration, the drug released from nanoparticles at w/w ratios 20:1 and 50:1 decreased. This may be due to increasing the polymer concentration that could form the

Table 3 Encapsulation Efficiency and Drug Loading of SPIONs

Sample Encapsulation Efficiency ±SD (%)		Drug Loading Content ±SD (%)
DOX-loaded PLA–PEG–FA SPIONs (10:1)	4.4±50.4	0.6±5.14
DOX-loaded PLA–PEG–FA SPIONs (20:1)	5.4±61.1	0.2±3.1
DOX-loaded PLA–PEG–FA SPIONs (50:1)	6.4±79.6	0.4±1.73

thicker polymer wall, which effectively prevented DOX from releasing in buffer.

In-vitro Cytotoxicity

Cytotoxicity of nanoparticles was investigated in HeLa (human cervix epithelial carcinoma cells) and CT26 (colon carcinoma cell) by MTT assay. As given in Figure 5, the free DOX decreased cell viability down to 52.94 ± 3.4% and 47.96 ± 3.4% at 24 hrs for HeLa and CT26 cell lines, respectively, whereas multifunctional nanoparticles with different w/w ratios can decrease cell viability down to 65.16 ± 5.8% and 61.38 ± 3.2% for HeLa and CT26 cell lines, respectively. The PLA–PEG–FA SPIONs (DOX free) at w/w ratio 10:1 showed much less toxicity with cell viability 82.83 ± 4.1% and 80.30 ± 2.1% for HeLa and CT26 cell lines, respectively. However, the PLA–PEG–FA SPIONs (DOX free) at w/w ratio 10:1 and DOX-loaded PLA–PEG–FA nanoparticles (SPIONs free) at 10:1 w/w ratio showed more cytotoxicity. The result indicates that the cytotoxicity was caused mainly by DOX itself. In comparison, the nanoparticles at w/w ratios of 20:1 and 50:1 showed more cell viability than those at w/w ratios of 10:1, because of slower DOX release profile (as mentioned above). On the other hand, cell viability was not significantly affected by the presence of SPIONs. The toxicity of the nanoparticles containing SPIONs were not significantly higher than nanoparticles without SPIONs. The toxicity of iron oxide was discussed in detail in a number of studies. It was reported that high concentrations of iron oxide nanoparticles induce cell necrosis. Most authors proposed that the mechanism of necrosis is associated with the generation of reactive oxygen species (ROS). The polymer shell reduces the toxic effects of nanoparticles containing SPIONs. The most likely mechanism for reducing cytotoxicity is the shielding of iron oxide nanocrystals from the intracellular environment.[51,63]

The Cellular Uptake and Apoptosis Study

The intracellular localization of DOX plays an important role in its anticancer activity. Therefore, localization of DOX in the HeLa and CT26 cell lines after incubation, with either free drug or drug loaded into multifunctional nanoparticles, were evaluated by fluorescence microscopy (Figure 6). A significant uptake of multifunctional nanoparticle was clearly observed from the red fluorescence image arising from DOX emission, suggesting that the drug-loaded nanoparticles were internalized in the cells.

To quantify the cellular uptake of prepared nanoparticles, flow cytometry analysis was carried out. Flow cytometry is

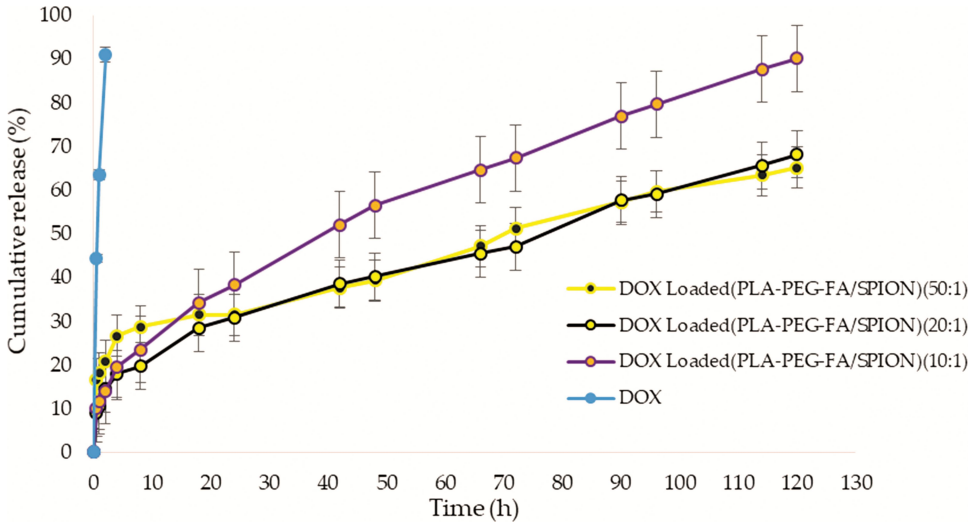

Figure 4 In-vitro release of free DOX and DOX-loaded PLA–PEG–FA SPIONs at various w/w ratios.

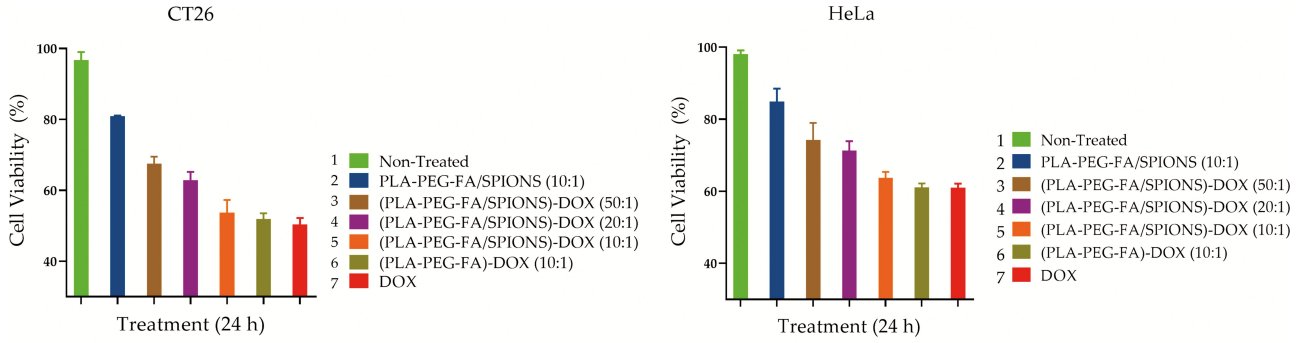

Treatment	1	2	3	4	5	6
2	****					
3	****	****				
4	****	****	ns			
5	****	****	****	**		
6	****	****	****	***	ns	
7	****	****	****	****	ns	ns

Treatment	1	2	3	4	5	6
2	***					
3	****	**				
4	****	***	ns			
5	****	****	**	*		
6	****	****	***	**	ns	
7	****	****	***	**	ns	ns

Figure 5 In-vitro cytotoxicity evaluation of DOX, DOX-loaded PLA–PEG–FA SPIONs with different w/w ratios, NPs without DOX and NPs without SPIONs in CT26 (left) and HeLa (right) cancer cells, (P-value: ns is Not-significance (≥ 0.05)., * is significant between 0.01 to 0.05, ** is significant between 0.001 to 0.01, *** is significant between 0.0001 to 0.001, and ****significant < 0.0001).

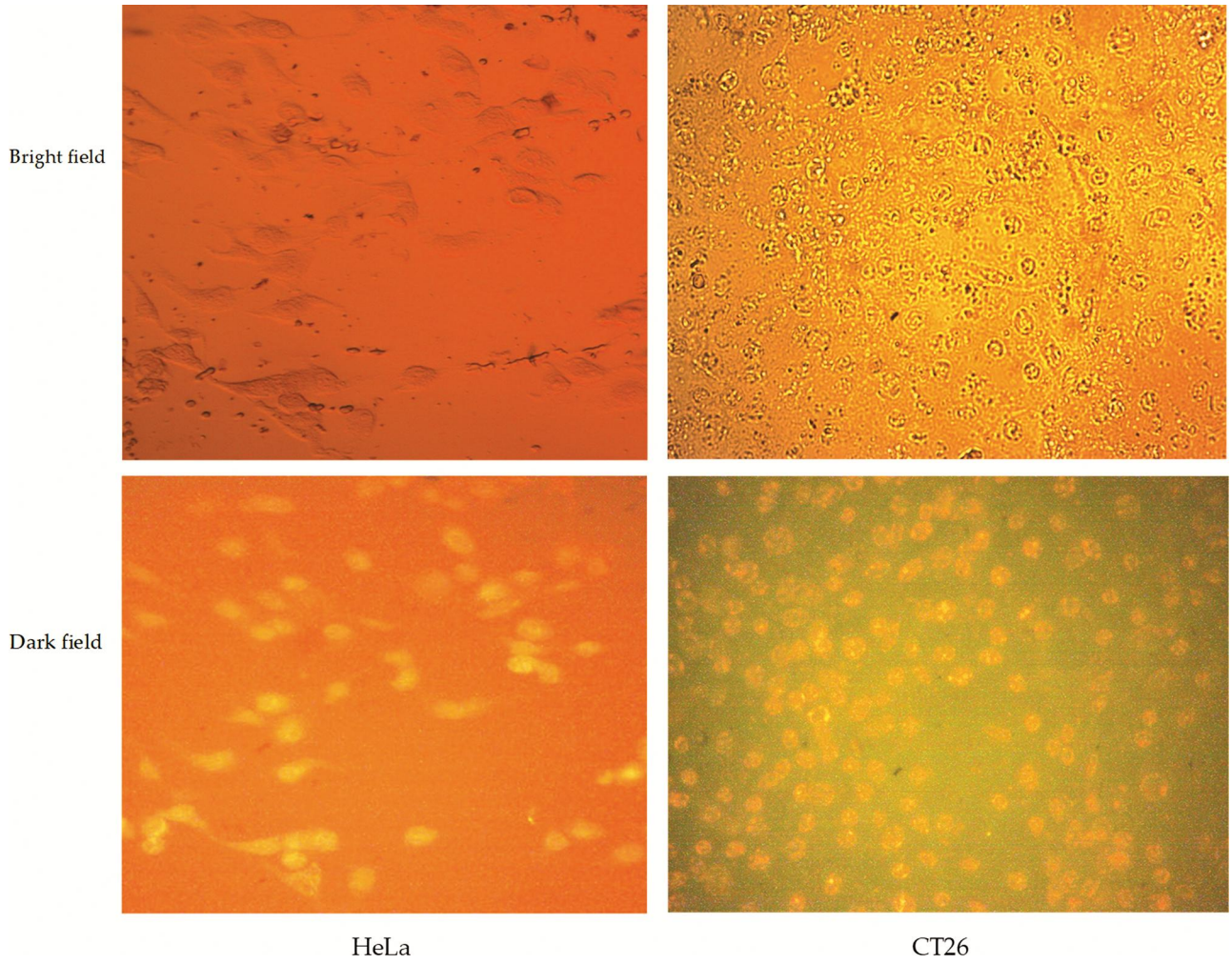

Figure 6 Fluorescence imaging of DOX-loaded PLA–PEG–FA SPIONs in (left) HeLa and (right) CT26 cells. Bright field (up) and dark field (down) for HeLa cells and CT26 cells.

a simple, rapid, and well-established method to quantify the viable cells in solution. Fluorescence microscopy and flow cytometry results showed that approximately all cells treated with free DOX and DOX-loaded PLA–PEG–FA SPIONs exhibit fluorescent signals. Therefore, the treatments were compared according to their mean fluorescence intensity of the internalized DOX complexes. Results showed that the cellular uptake of DOX-loaded PLA–PEG–FA SPIONs were significantly higher than those of DOX-loaded PLA–PEG SPIONs (nanoparticles without folic acid). The cellular uptake efficiency of DOX-loaded PLA–PEG–FA SPIONs were more than (3.5-fold) to that of DOX-loaded PLA–PEG–SPIONs (nanoparticles without folic acid) in both cell lines, as shown in Figure 7. This observation may be related to the higher uptake of targeted nanoparticles into the cells due to their receptor-mediated endocytosis. A higher cellular uptake of targeted nanoparticles than non-targeted ones was observed in CT26 cells in comparison to those in HeLa cells. This issue may be related to the higher expression of folate receptors in CT26 cells compared to HeLa cells. This would highlight the prominent role of folic acid ligand in the cellular uptake efficiency.[9] It was also noticeable that the cellular uptake efficiency of DOX-loaded PLA–PEG–FA SPIONs were approximately similar to that of DOX-loaded PLA–PEG–FA nanoparticles (SPIONs free) for HeLa and CT26 cell lines. However, despite the slightly higher mean fluorescence intensity observed in the cellular uptake of DOX-loaded PLA–PEG–FA SPIONs than those of DOX-loaded PLA–PEG–FA nanoparticles (SPIONs free), the statistical evaluation showed no significance difference between them ($p \leq 0.05$).

In order to compare the strength of the apoptotic effect in DOX and DOX-loaded PLA–PEG–FA SPIONs, flow cytometry analysis of Annexin V-FITC was performed (Figure 8). Annexin V-FITC staining can distinguish early apoptosis from late apoptosis or living cells from necrotic cells. To examine DOX and DOX-loaded PLA–PEG–FA SPIONs induced apoptosis in HeLa and CT26 cells quantitatively, the cells were exposed to DOX and DOX-loaded PLA–PEG–FA SPIONs with w/w ratio 10:1 for 24 hrs, and the percentage of cell apoptosis was determined by flow cytometry analysis. The percentage of apoptosis of DOX-treated cells was 48.2 ± 2.8% and 56.7 ± 3.5% within 24 hrsfor HeLa and CT26 cell lines, respectively. However, a higher percentage of dead cells were observed when cells were treated with DOX-loaded PLA–PEG–FA SPIONs. The percentage of apoptotic cells reached 57.75± 3.8% and 61.81± 4.1% after 24 hrs for

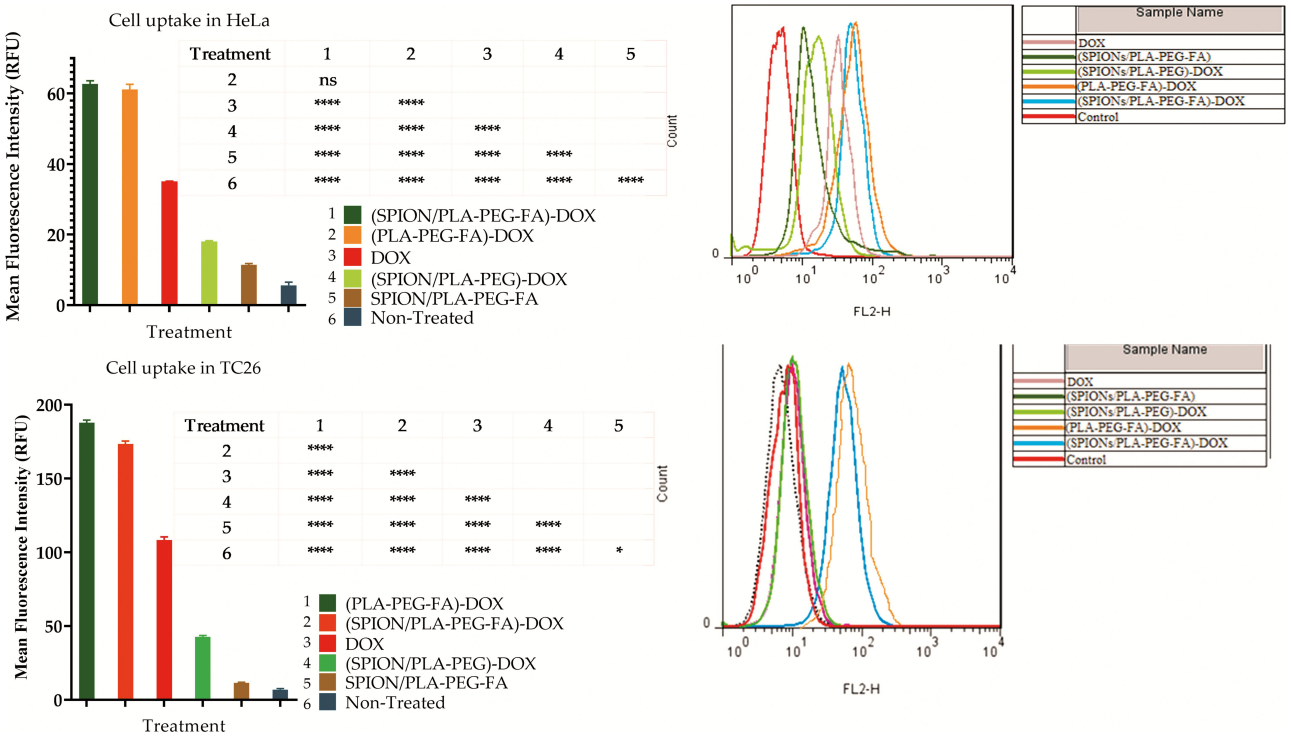

Figure 7 Cellular uptake of the free DOX and DOX-loaded PLA–PEG–FA SPIONs in (up) HeLa and (down) CT26 cells. (P-value: ns is not-significance (≥ 0.05)., * is significant between 0.01 to 0.05., and ****significant < 0.0001).

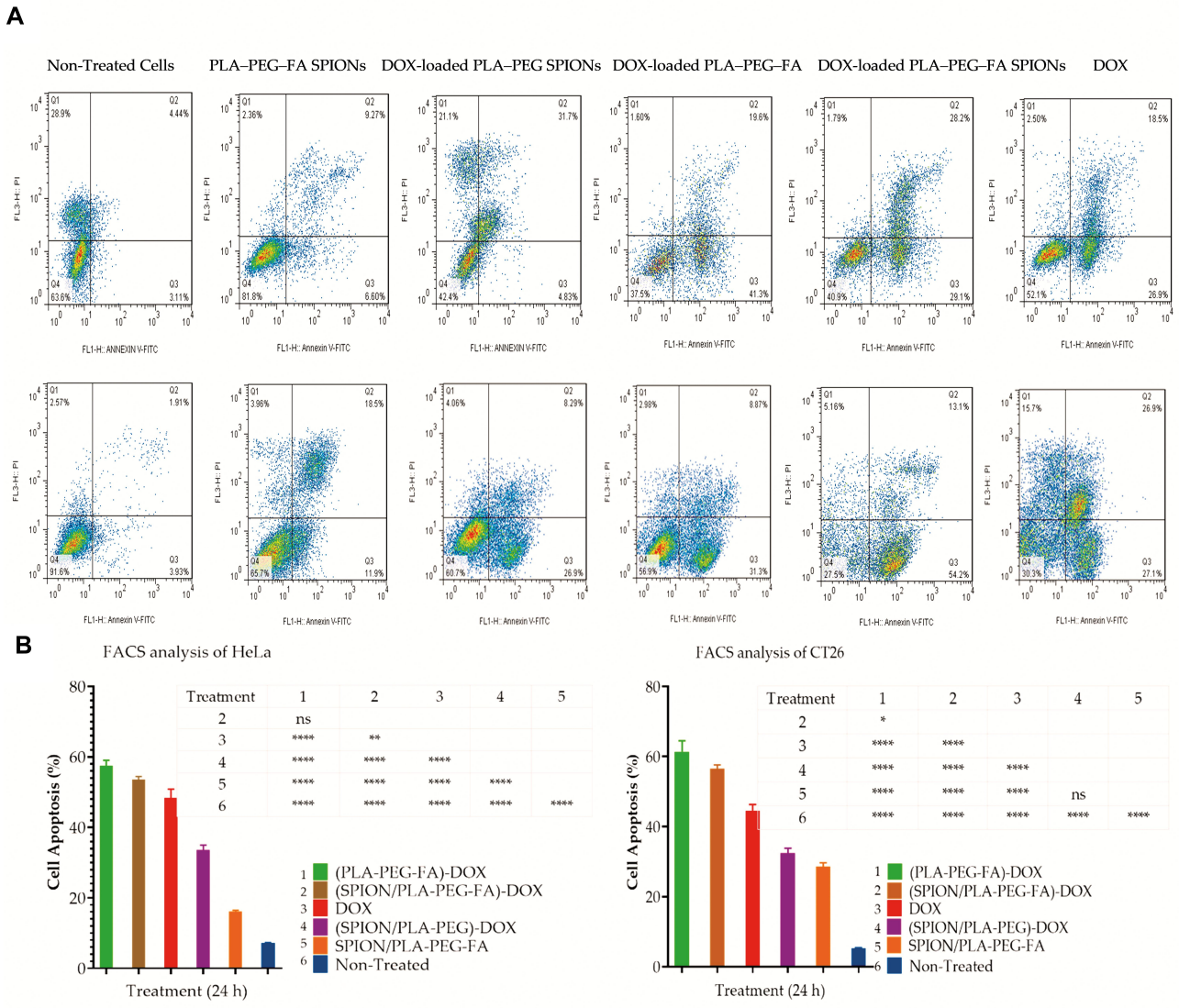

Figure 8 Cell Apoptosis: (**A**) Flow cytometry histograms of (up) HeLa and (down) CT26 treated with DOX and different forms of DOX-loaded PLA–PEG–FA SPIONs for 24h and then stained with propidium iodine and Annexin V-FITC, (Q1: dead cells with Annexin V-FITC (-)/PI (+), Q2: late apoptotic cells with Annexin V-FITC (+)/PI (+) Q3: live cells with AnnexinV-FITC (-)/PI (-), Q4: early apoptotic cells with Annexin V-FITC (+)/PI (-)) and (**B**) the number of apoptosis cells was counted with a FACS Calibur flow cytometer for HeLa (left) and CT26 (right) cells. (P-value: ns is not-significance (≥ 0.05)., * is significant between 0.01 to 0.05., ** is significant between 0.001 to 0.01., and ****, significant < 0.0001).

HeLa and CT26 cell lines, respectively. The results indicate that DOX-loaded PLA–PEG–FA SPIONs induce higher cytotoxicity rate and cellular uptake on these cancer cells compared to those of DOX-loaded PLA–PEG SPIONs (non-targeted) and free DOX. In agreement with the results obtained, several reports showed that targeted nanoparticles yield higher cellular uptake and apoptosis than free DOX. It is reported that cellular uptake of nanoparticles happens via endocytosis process, while free DOX in the form of water-soluble molecules was internalized in the cell via passive diffusion.[64] Therefore, the entry of DOX molecules into the cell via passive diffusion may be easier and faster than the endocytosis of DOX-loaded PLA–PEG nanoparticles (non-targeted). On the other hand, For DOX-loaded PLA–PEG–FA SPIONs (targeted form), folic acid improved the specific binding to the folate receptor overexpressed on HeLa and CT26 cell surfaces. This binding facilitated folate receptor-mediated endocytosis resulting in better cellular uptake of DOX-loaded PLA–PEG–FA SPIONs and subsequently increase apoptosis. Also, the viability levels of DOX-loaded PLA–PEG SPIONs (non-targeted) treated cells were similar for both cell lines (33.81± 1.8% and 32.03± 1.1% for HeLa and CT26 cell lines, respectively). This result is due to the fact that cellular uptake of non-targeted nanoparticles was not facilitated by folate receptor-mediated endocytosis.

Conclusions

Nowadays, there are several different types of cancer treatment. The efficacy of monotherapies has been limited due to intra-tumor heterogeneity. Combination therapies in cancer show enhanced efficacy via additive or synergistic anticancer effects. Hyperthermia has been demonstrated to offer numerous advantages when integrated with chemotherapy in nano-platforms, such as increased accumulation of drugs in the tumor site, enhanced cellular uptake, inhibition of DNA repair, and accelerated drug cytotoxicity against cancer cells. These evidences suggest a promising anticancer synergistic effect of hyperthermia and chemotherapy. The targeted delivery of hyperthermic SPIONs and anticancer drug (DOX) to a specific target site with minimum side effects is an important challenge in targeted Hyperthermia-chemotherapy.

In the present study, DOX-loaded PLA–PEG–FA SPIONs were prepared and drug release behavior, heat production capacity upon AMF, cellular uptake efficiency and apoptotic effects were investigated. The results showed that DOX released gradually from DOX-loaded PLA–PEG–FA SPIONs (About 90% of the total DOX was gradually released during 120 hrs in w/w ratio 10:1). Moreover, these multifunctional nanoparticles demonstrated significant heat generation capability (44.2° C in w/w ratio 10:1), which is remarkably sufficient for the destruction of cancer cells.

The results indicated that cellular uptake of DOX-loaded PLA–PEG–FA SPIONs were higher than that of DOX-loaded PLA–PEG SPIONs (non-targeted) and free DOX. Subsequently, an increase in the rate of apoptosis was observed in DOX-loaded PLA–PEG–FA SPIONs compared to DOX-loaded PLA–PEG SPIONs (non-targeted) and free DOX (The percentage of apoptotic cells reached 57.75± 3.8% and 61.81± 4.1% after 24 hrs for HeLa and CT26 cell lines, respectively). Therefore, DOX-loaded PLA–PEG–FA SPIONs can be used as a tumor-targeting multifunctional delivery system for targeted hyperthermia-chemotherapy of cancer cells.

Disclosure

The authors report no conflicts of interest in this work.

References

1. Pucci C, Martinelli C, Ciofani G. Innovative approaches for cancer treatment: current perspectives and new challenges. *Ecancermedicalscience*. 2019;13.
2. Kakde D, Jain D, Shrivastava V, Kakde R, Patil A. Cancer therapeutics-opportunities, challenges and advances in drug delivery. *J Appl Pharma Sci*. 2011;1(9):1–10.
3. Zabarjadi A, Hashemzadeh H, Taravat E. Telomere, chromosome end and telomerase enzyme as a cancer biomarker. *Genet Third Millenn*. 2013;11(1):3019–3027.
4. Chidambaram M, Manavalan R, Kathiresan K. Nanotherapeutics to overcome conventional cancer chemotherapy limitations. *J Pharm Pharm Sci*. 2011;14(1):67–77. doi:10.18433/J30C7D
5. Senapati S, Mahanta AK, Kumar S, Maiti P. Controlled drug delivery vehicles for cancer treatment and their performance. *Signal Transduct Targeted Ther*. 2018;3(1):1–19. doi:10.1038/s41392-017-0004-3
6. Zhang B, Wan S, Peng X, et al. Human serum albumin-based doxorubicin prodrug nanoparticles with tumor ph-responsive aggregation-enhanced retention and reduced cardiotoxicity. *J Mater Chem B*. 2020;8(17):3939–3948. doi:10.1039/D0TB00327A
7. Babincová M, Durdík Š, Babincová N, Sourivong P, Babinec P. Application of cationized magnetoferritin for magnetic field-assisted delivery of short interfering RNA in vitro. *Lasers Med Sci*. 2018;33(8):1807–1812. doi:10.1007/s10103-018-2547-0
8. Siminzar P, Omidi Y, Golchin A, Aghanejad A, Barar J. Targeted delivery of doxorubicin by magnetic mesoporous silica nanoparticles armed with mucin-1 aptamer. *J Drug Target*. 2020;28(1):92–101. doi:10.1080/1061186X.2019.1616745
9. Darvishi MH, Nomani A, Hashemzadeh H, Amini M, Shokrgozar MA, Dinarvand R. Targeted DNA delivery to cancer cells using a biotinylated chitosan carrier. *Biotechnol Appl Biochem*. 2017;64(3):423–432. doi:10.1002/bab.1497
10. Razavi H, Darvishi MH, Janfaza S. Silver sulfadiazine encapsulated in lipid-based nanocarriers for burn treatment. *J Burn Care Res*. 2018;39(3):319–325.
11. Darvishi MH, Nomani A, Amini M, Shokrgozar MA, Dinarvand R. Novel biotinylated chitosan-graft-polyethyleneimine copolymer as a targeted non-viral vector for anti-EGF receptor siRNA delivery in cancer cells. *Int J Pharm*. 2013;456(2):408–416. doi:10.1016/j.ijpharm.2013.08.069
12. Khafaji M, Zamani M, Vossoughi M, Iraji Zad A. Doxorubicin/cisplatin-loaded superparamagnetic nanoparticles as a stimuli-responsive co-delivery system for chemo-photothermal therapy. *Int J Nanomedicine*. 2019;14:8769. doi:10.2147/IJN.S226254
13. Jafari S, Mahyad B, Hashemzadeh H, Janfaza S, Gholikhani T, Tayebi L. Biomedical applications of tio2 nanostructures: recent advances. *Int J Nanomedicine*. 2020;15:3447. doi:10.2147/IJN.S249441
14. Singh R, Lillard JW. Nanoparticle-based targeted drug delivery. *Exp Mol Pathol*. 2009;86(3):215–223. doi:10.1016/j.yexmp.2008.12.004
15. Arruebo M, Vilaboa N, Sáez-Gutierrez B, et al. Assessment of the evolution of cancer treatment therapies. *Cancers*. 2011;3(3):3279–3330. doi:10.3390/cancers3033279
16. Hashemzadeh H, Javadi H, Darvishi MH. Study of structural stability and formation mechanisms in DSPC and DPSM liposomes: A coarse-grained molecular dynamics simulation. *Sci Rep*. 2020;10(1):1837. doi:10.1038/s41598-020-58730-z
17. Wang Z, Yu L, Ding M, Tan H, Li J, Fu Q. Preparation and rapid degradation of nontoxic biodegradable polyurethanes based on poly (lactic acid)-poly (ethylene glycol)-poly (lactic acid) and l-lysine diisocyanate. *Polym Chem*. 2011;2(3):601–607. doi:10.1039/C0PY00235F
18. Singhvi M, Zinjarde S, Gokhale D. Polylactic acid: synthesis and biomedical applications. *J Appl Microbiol*. 2019;127(6):1612–1626. doi:10.1111/jam.14290
19. Song R, Murphy M, Li C, Ting K, Soo C, Zheng Z. Current development of biodegradable polymeric materials for biomedical applications. *Drug Des Devel Ther*. 2018;12:3117. doi:10.2147/DDDT.S165440

20. D'souza AA, Shegokar R. Polyethylene glycol (peg): A versatile polymer for pharmaceutical applications. *Expert Opin Drug Deliv*. 2016;13(9):1257–1275. doi:10.1080/17425247.2016.1182485
21. Suk JS, Xu Q, Kim N, Hanes J, Ensign LM. Pegylation as a strategy for improving nanoparticle-based drug and gene delivery. *Adv Drug Deliv Rev*. 2016;99:28–51. doi:10.1016/j.addr.2015.09.012
22. Zhou J, Rossi JJ. Cell-specific aptamer-mediated targeted drug delivery. *Oligonucleotides*. 2011;21(1):1–10. doi:10.1089/oli.2010.0264
23. Modrejewski J, Walter J-G, Kretschmer I, et al. Aptamer-modified polymer nanoparticles for targeted drug delivery. *BioNanoMaterials*. 2016;17(1–2):43–51. doi:10.1515/bnm-2015-0027
24. Awwad S, Angkawinitwong U. Overview of antibody drug delivery. *Pharmaceutics*. 2018;10(3):83. doi:10.3390/pharmaceutics10030083
25. Kennedy PJ, Oliveira C, Granja PL, Sarmento B. Antibodies and associates: partners in targeted drug delivery. *Pharmacol Ther*. 2017;177:129–145. doi:10.1016/j.pharmthera.2017.03.004
26. Vrettos EI, Mező G, Tzakos AG. On the design principles of peptide–drug conjugates for targeted drug delivery to the malignant tumor site. *Beilstein J Org Chem*. 2018;14(1):930–954. doi:10.3762/bjoc.14.80
27. Chen S, Zhao X, Chen J, et al. Mechanism-based tumor-targeting drug delivery system. Validation of efficient vitamin receptor-mediated endocytosis and drug release. *Bioconjug Chem*. 2010;21(5):979–987. doi:10.1021/bc9005656
28. Nosrati H, Barzegari P, Danafar H, Kheiri Manjili H. Biotin-functionalized copolymeric PEG-PCL micelles for in vivo tumour-targeted delivery of artemisinin. *Artif Cell Nanomed Biotechnol*. 2019;47(1):104–114. doi:10.1080/21691401.2018.1543199
29. Russell-Jones G, McTavish K, McEwan J, Rice J, Nowotnik D. Vitamin-mediated targeting as a potential mechanism to increase drug uptake by tumours. *J Inorg Biochem*. 2004;98(10):1625–1633. doi:10.1016/j.jinorgbio.2004.07.009
30. Zhao X, Li H, Lee RJ. Targeted drug delivery via folate receptors. *Expert Opin Drug Deliv*. 2008;5(3):309–319. doi:10.1517/17425247.5.3.309
31. Mansouri S, Cuie Y, Winnik F, et al. Characterization of folate-chitosan-DNA nanoparticles for gene therapy. *Biomaterials*. 2006;27(9):2060–2065. doi:10.1016/j.biomaterials.2005.09.020
32. Daglioglu C. Environmentally responsive dual-targeting nanoparticles: improving drug accumulation in cancer cells as a way of preventing anticancer drug efflux. *J Pharm Sci*. 2018;107(3):934–941. doi:10.1016/j.xphs.2017.10.029
33. Sunoqrot S, Bugno J, Lantvit D, Burdette JE, Hong S. Prolonged blood circulation and enhanced tumor accumulation of folate-targeted dendrimer-polymer hybrid nanoparticles. *J Control Release*. 2014;191:115–122. doi:10.1016/j.jconrel.2014.05.006
34. Hami Z, Amini M, Ghazi-Khansari M, Rezayat SM, Gilani K. Doxorubicin-conjugated PLA-PEG-folate based polymeric micelle for tumor-targeted delivery: synthesis and in vitro evaluation. *DARU J Pharm Sci*. 2014;22(1):30. doi:10.1186/2008-2231-22-30
35. Wakharde A, Awad A, Bhagat A, Karuppayil S. Synergistic activation of doxorubicin against cancer: A review. *Am J Clin Microbiol Antimicrob*. 2018;1(2):1009.
36. Melguizo C, Cabeza L, Prados J, et al. Enhanced antitumoral activity of doxorubicin against lung cancer cells using biodegradable poly (butyl-cyanoacrylate) nanoparticles. *Drug Des Devel Ther*. 2015;9:6433.
37. Abandansari RM, Parsian H, Kazerouni F, Porbagher R, Zabihi E, Rahimipour A. Effect of simultaneous treatment with royal jelly and doxorubicin on the survival of the prostate cancer cell line (pc3): an in vitro study. *Int J Cancer Manage*. 2018;11(4).
38. Prados J, Melguizo C, Ortiz R, et al. Doxorubicin-loaded nanoparticles: new advances in breast cancer therapy. *Anti Cancer Agent Med Chem*. 2012;12(9):1058–1070.
39. Singh AP, Biswas A, Shukla A, Maiti P. Targeted therapy in chronic diseases using nanomaterial-based drug delivery vehicles. *Signal Transduct Targeted Ther*. 2019;4(1):1–21. doi:10.1038/s41392-019-0068-3
40. Gomari H, Moghadam MF, Soleimani M, Ghavami M, Khodashenas S. Targeted delivery of doxorubicin to her2 positive tumor models. *Int J Nanomedicine*. 2019;14:5679. doi:10.2147/IJN.S210731
41. Mirzaei-Kalar Z, Yavari A, Jouyban A. Increasing DNA binding affinity of doxorubicin by loading on fe3o4 nanoparticles: A multi-spectroscopic study. *Spectrochim Acta A Mol Biomol Spectrosc*. 2020;229:117985. doi:10.1016/j.saa.2019.117985
42. Canela VC, Crivelaro CN, Ferla LZ, et al. Synergistic effects of combined therapy: nonfocused ultrasound plus aussie current for noninvasive body contouring. *Clin Cosmet Investig Dermatol*. 2018;11:203. doi:10.2147/CCID.S157782
43. Christie C, Molina S, Gonzales J, et al. Synergistic chemotherapy by combined moderate hyperthermia and photochemical internalization. *Biomed Opt Express*. 2016;7(4):1240–1250. doi:10.1364/BOE.7.001240
44. Luk KH, Hulse RM, Phillips TL. Hyperthermia in cancer therapy. *West J Med*. 1980;132(3):179.
45. Baronzio G, Parmar G, Ballerini M, Szasz A, Baronzio M, Cassutti V. A brief overview of hyperthermia in cancer treatment. *J Integr Oncol*. 2014;3(115):2. doi:10.4172/2329-6771.1000115
46. Babincová N, Sourivong P, Babinec P, Bergemann C, Babincová M, Durdík Š. Applications of magnetoliposomes with encapsulated doxorubicin for integrated chemotherapy and hyperthermia of rat c6 glioma. *Z Für Naturfor C*. 2018;73(7–8):265–271. doi:10.1515/znc-2017-0110
47. Liu D, Hong Y, Li Y, et al. Targeted destruction of cancer stem cells using multifunctional magnetic nanoparticles that enable combined hyperthermia and chemotherapy. *Theranostics*. 2020;10(3):1181. doi:10.7150/thno.38989
48. Wust P, Hildebrandt B, Sreenivasa G, et al. Hyperthermia in combined treatment of cancer. *Lancet Oncol*. 2002;3(8):487–497. doi:10.1016/S1470-2045(02)00818-5
49. Berry CC, Curtis AS. Functionalisation of magnetic nanoparticles for applications in biomedicine. *J Phys D: Appl Phys*. 2003;36(13):R198. doi:10.1088/0022-3727/36/13/203
50. Zhang G, Liao Y, Baker I. Surface engineering of core/shell iron/iron oxide nanoparticles from microemulsions for hyperthermia. *Mater Sci Eng*. 2010;30(1):92–97. doi:10.1016/j.msec.2009.09.003
51. Mahmoudi M, Sant S, Wang B, Laurent S, Sen T. Superparamagnetic iron oxide nanoparticles (SPIONs): development, surface modification and applications in chemotherapy. *Adv Drug Deliv Rev*. 2011;63(1–2):24–46. doi:10.1016/j.addr.2010.05.006
52. Yang X, Grailer JJ, Rowland IJ, et al. Multifunctional SPIO/DOX-loaded wormlike polymer vesicles for cancer therapy and MR imaging. *Biomaterials*. 2010;31(34):9065–9073. doi:10.1016/j.biomaterials.2010.08.039
53. Kim DK, Mikhaylova M, Zhang Y, Muhammed M. Protective coating of superparamagnetic iron oxide nanoparticles. *Chem Mater*. 2003;15(8):1617–1627. doi:10.1021/cm021349j
54. Patil YB, Toti US, Khdair A, Ma L, Panyam J. Single-step surface functionalization of polymeric nanoparticles for targeted drug delivery. *Biomaterials*. 2009;30(5):859–866. doi:10.1016/j.biomaterials.2008.09.056
55. Shah RR, Davis TP, Glover AL, Nikles DE, Brazel CS. Impact of magnetic field parameters and iron oxide nanoparticle properties on heat generation for use in magnetic hyperthermia. *J Magn Magn Mater*. 2015;387:96–106. doi:10.1016/j.jmmm.2015.03.085
56. Razavi S, Partoazar A, Takzaree N, Fasihi-Ramandi M, Bahador A, Darvishi MH. Silver sulfadiazine nanoethogel for burn healing: characterization and investigation of its in vivo effects. *Nanomedicine*. 2018;13(11):1319–1331. doi:10.2217/nnm-2017-0385
57. Ghasemi R, Abdollahi M, Zadeh EE, et al. mPEG-PLA and PLA-PEG-PLA nanoparticles as new carriers for delivery of recombinant human growth hormone (rhGH). *Sci Rep*. 2018;8(1):1–13. doi:10.1038/s41598-018-28092-8

58. Mourdikoudis S, Pallares RM, Thanh NT. Characterization techniques for nanoparticles: comparison and complementarity upon studying nanoparticle properties. *Nanoscale*. 2018;10(27):12871–12934.
59. Behzadi S, Serpooshan V, Tao W, et al. Cellular uptake of nanoparticles: journey inside the cell. *Chem Soc Rev*. 2017;46 (14):4218–4244.
60. Li Z, Kawashita M, Araki N, Mitsumori M, Hiraoka M, Doi M. Magnetite nanoparticles with high heating efficiencies for application in the hyperthermia of cancer. *Mater Sci Eng*. 2010;30(7):990–996. doi:10.1016/j.msec.2010.04.016
61. Taratula O, Dani RK, Schumann C, et al. Multifunctional nanomedicine platform for concurrent delivery of chemotherapeutic drugs and mild hyperthermia to ovarian cancer cells. *Int J Pharm*. 2013;458 (1):169–180. doi:10.1016/j.ijpharm.2013.09.032
62. Fu Y, Kao WJ. Drug release kinetics and transport mechanisms of non-degradable and degradable polymeric delivery systems. *Expert Opin Drug Deliv*. 2010;7(4):429–444. doi:10.1517/17425241003602259
63. Kumar CS, Mohammad F. Magnetic nanomaterials for hyperthermia-based therapy and controlled drug delivery. *Adv Drug Deliv Rev*. 2011;63(9):789–808. doi:10.1016/j.addr.2011.03.008
64. Salatin S, Yari Khosroushahi A. Overviews on the cellular uptake mechanism of polysaccharide colloidal nanoparticles. *J Cell Mol Med*. 2017;21(9):1668–1686. doi:10.1111/jcmm.13110